AUT Journal of Electrical Engineering

AUT J. Electr. Eng., 55(1) (2023) 3-10
DOI: 10.22060/eej.2022.20591.5437

A Wideband Transmitarray Antenna Design Based on the Transmission Characteristic of the UnitCell

Mohammad Reza Salimi Beni, Mohammad Zoofaghari *

Department of Electrical Engineering, Yazd University, Yazd, Iran

ABSTRACT: In this paper, a procedure is proposed to design a wideband transmitarray upon a specified frequency band. In this way, the phase control parameter of a unit cell is adjusted in a suggested range, ensuring linear phase change and low transmission loss over the band. The unit cell is designed for a range of phase control parameters (e.g., slot length in a CSRR), in which a 360° phase variation is provided. Part of this range is applied for the central elements of TA, in which the maximum overlapped passband (for different values of phase control parameter) around the desired frequency is to be achieved. In this way, a scenario for the phase specification of the array elements would be obtained. This range is specially applied for the central elements of the array, which are in exposure to feed peak power. As a proof of this concept, a 14×14 element transmitarray is designed and fabricated based on a back-to-back square Complementary Split-Ring Resonator (CSRR). Measurement results indicate maximum gain, 1-dB bandwidth, and aperture efficiency of 24.6 dB, 18.4%, and 53% respectively, at the center frequency of 11.5GHz. At the end of the paper, a comparison between the proposed TA and the previous ones is provided.

Review History:

Received: Sep.24, 2021
Revised: May, 08, 2022
Accepted: Jun. 21, 2022
Available Online: Mar. 01, 2023

Keywords:

Transmitarray
Split Ring Resonator
Frequency Selective Surface
Unit Cell

1- Introduction

The advantages of Transmitarray Antenna (TA), such as high gain, simplicity, low cost of implementation, and beamforming capabilities have been revealed in the recent research. TAs are an appropriate alternative for large bulky lens antennas, especially at low frequencies in a wide spectrum of applications, including radar technologies and high-gain steerable antenna arrays for new generations of telecommunication (e.g., 5G). Transmitarrays are fittingly-integrated in MMIC for millimeter-wave radar sensors. Additionally, as the beamforming is provided by the special shape and dimension of the unit cells, a TA could be well adapted to the conformal geometries.

The array elements are supposed to effectively steer the radiation beam of the feed toward the desired direction through the compensation of phase shift due to their various distances from the feed. Thus, for a wideband TA, the unit cell needs to have a low transmission loss and a transmission phase adjustable in a range of 360° through a phase control geometry parameter upon a wide range of frequencies. In many cases, a multi-layer structure is exploited to fulfill 360° phase range criteria. The elements of the wideband array need to be designed to perform the phase compensation linearly proportional to the frequency, owing to their electrical distance to the feed. Conducted studies in this area mainly address the bandwidth enhancement by increasing the bandwidth of array elements or unit cell phase range [1-11].

A four-layer double split-ring slot element has been used in [1] to achieve 7.4% 1-dB gain bandwidth. The array elements in [1] have low transmission loss as well as low sensitivity to the incidence angle. Abdelrahman et. al exploited a triple-layer spiral dipole element for TA, which yields 1-dB gain bandwidth of 9% [2]. This was an improvement toward the previously reported structures. However, variation of the spiral dipole length cannot fulfill the linear 360° phase range. In [3], the design, implementation, and comparison of two different TAs using polarization-insensitive elements have been presented.

A three-layer, slot-based, unit cell without dielectric has been developed in [4], in which some stubs are applied to control the notch frequency of the TA passband. An extremely high aperture efficiency of 55% has been obtained due to a suitable feed horn along with mitigation of dielectric loss. 1-dB gain bandwidth of 15.5% is another advantage of the suggested TA. However, this TA suffers from non-linearity of phase-stubs length and phase-frequency curves in which no more than 21% 3-dB gain bandwidth is acquired.

A three-layer FSS has been designed and fabricated by Luo et. al in which the layers are separated by quarter-wavelength air gaps [5]. The unit cell includes a square slot

*Corresponding author's email: zoofaghari@gmail.com

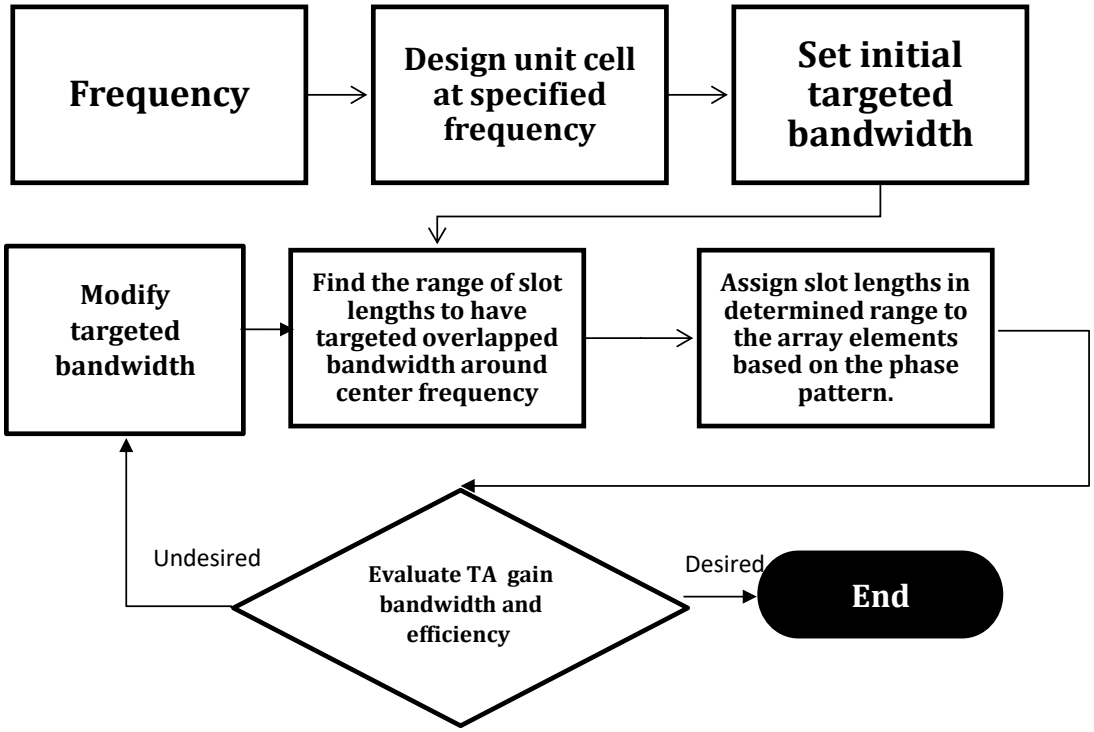

Fig. 1. flowchart of the proposed TA design approach

loaded with four strips at the mid-layer, sandwiched by a pair of square patches on the top and bottom layers. 1-dB gain bandwidth of 16% and aperture efficiency of 60% were reported, which are extremely high values in comparison with similar previous TAs. Nevertheless, a full 360° phase range is not satisfied within the transmission passband of the element.

Abdelrahman et. al addresses a method to increase the bandwidth through the control of transmission phase range and the optimization of phase distribution on TA aperture [6]. While an extremely high maximum gain of 29.3 dB is obtained, 1-dB bandwidth is not more than 11.7%.

In [7], a double conformal ring is utilized as the unit cell, where a phase coverage of up to 600° is achieved. However, 1-dB bandwidth is not more than 7%.

A low-profile and wideband TA antenna is presented in [8], which comprises three-layer elements in which the top and bottom layers consist of square patches, and the middle layer of the Jerusalem slot. The proposed unit cell indicates suitable transmission characteristics.

A semi-planar structure for TA antennas is suggested by Ramazannia Tuloti et. al [9]. Due to the geometrical curvature of this array, the required transmission phase range is reduced substantially from 360°, resulting in improved bandwidth and efficiency.

A novel two-layer element connected by a metal post is introduced in [10] that provides a 360° phase shift, low insertion loss, and a wide bandwidth.

Additionally, Feng et. al demonstrates an ultrawideband TA fed by a Vivaldi array that indicates a stable radiation pattern and reasonable SLL in 5-19 GHz [11].

For a wideband TA, we need low transmission loss, especially for the centrally located elements over the whole frequency band to avoid gain bandwidth degradation as well. To this end, the passband of the unit cell for different values of phase control parameter must be adjusted inside the desired band. This imposes some extra constraints on the geometry parameters of the unit cell. Sequential steps are introduced for a TA design in a way that is different from some pervious work [12].

This approach is employed here to realize a TA based on a multi-layer back-to-back complementary square ring resonator as the unit cell whose phase is controlled by the slot length.

A TA including 14×14 elements is designed and fabricated utilizing the introduced CSRR. Low cross-polarization is observed in measured patterns of the array due to the single-polarization essence of the proposed unit cell. The results for this TA are compared with those reported in previous works at the end of this paper.

In the following, first the general aspects of the proposed design procedure are introduced and the unit cell and array design are presented and discussed in two separate sections. Finally, the measured pattern, as well as gain and aperture efficiency, would be illustrated vs. frequency.

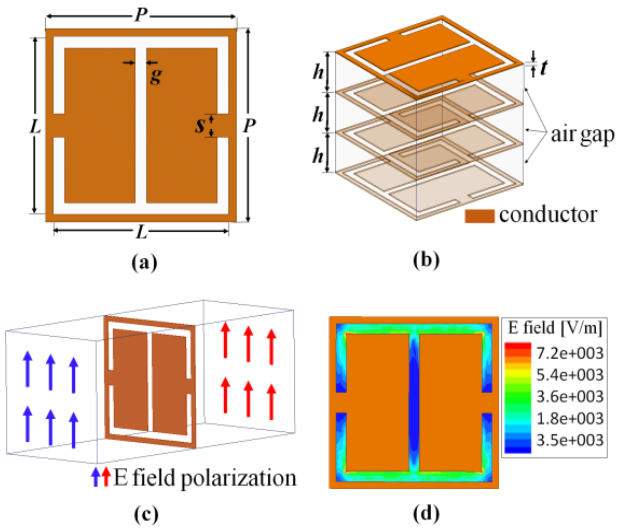

Fig. 2. Structure of proposed CSRR including (a) geometry of each layer, (b) layers configuration, (c) the unit cell in the exposure of the incident electric field, and (d) colormap of the induced tangential electric field on the slot

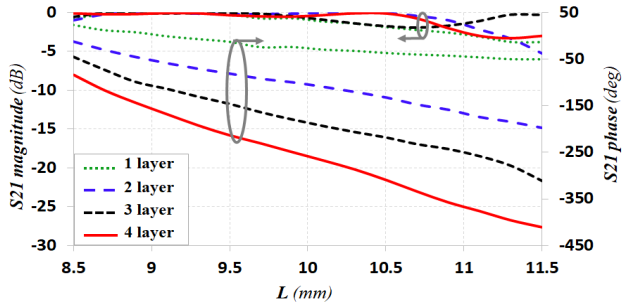

Fig. 3. Magnitude and phase of transmission coefficient in terms of slot length for different number of layers

2- Proposed TA Design Approach

The proposed procedure for a wideband TA design is clarified in this section as shown in the flowchart (Fig.1). According to this diagram, in the first step, the unit cell is designed for a specified frequency and its parameters are obtained to get the maximum bandwidth.

Considering an initially targeted bandwidth based on frequency characteristics of the realized unit cell, we obtain a range for phase control parameter (e.g., slot length in a CSRR), for which the targeted overlapped passband (for different values of phase control parameter) around the desired frequency is achieved. Fortunately, the cell also fulfills a linear phase upon this band similar to the passband of an ordinary RLC filter. Consequently, the more the bandwidth of the unit cell for each parameter value, the more the bandwidth of the overlapped passband and the more the bandwidth of TA.

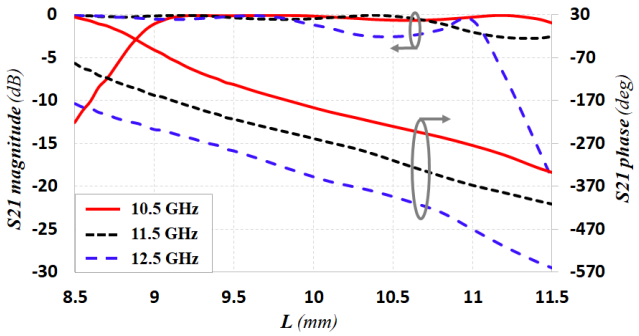

Fig. 4. Magnitude and phase of transmission coefficient in terms of slot length for various frequencies of the passband

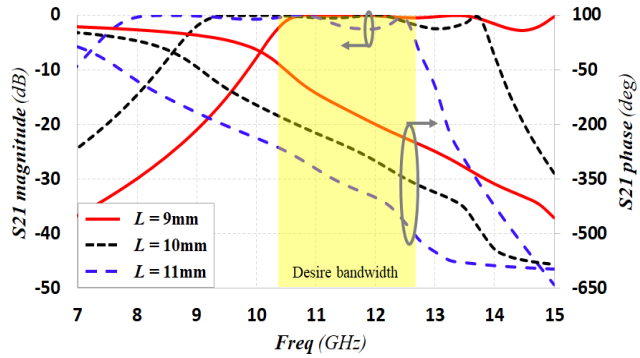

Fig. 5. Magnitude and phase of transmission coefficient in terms of frequency for l=9mm, l=10mm, and, l=11mm

Afterwards, slot lengths of the already determined range are assigned to the array elements based on the phase pattern. It is important to allocate the slot lengths that provide a more symmetric passband (around the desired frequency) to the cells at the central positions in the array.

Finally, the gain bandwidth and the aperture efficiency of the implemented TA are assessed. In this step, the targeted bandwidth might need to be modified iteratively, where after each modification, the slot lengths are re-determined and the array is re-designed to achieve the desired TA performance.

3- Unit Cell Design

The proposed four-layer CSRR is depicted in Fig. 2. This structure has no substrate, which reduces the fabrication cost and makes it suitable for high power applications. Considering the central frequency of 11.5GHz, the unit cell is to be designed to maximize the overlapped passband around 11.5GHz for various slot lengths, L.

Fig. 3 represents the phase curves of CSRR for a different number of layers. The single-layer structure requires a wide range of slot lengths to cover the full 360° phase range that causes overlapped bandwidth reduction. Thus, four layers spaced by an air gap of thickness h are adapted for the proposed CSRR in this paper (see Fig. 2b).

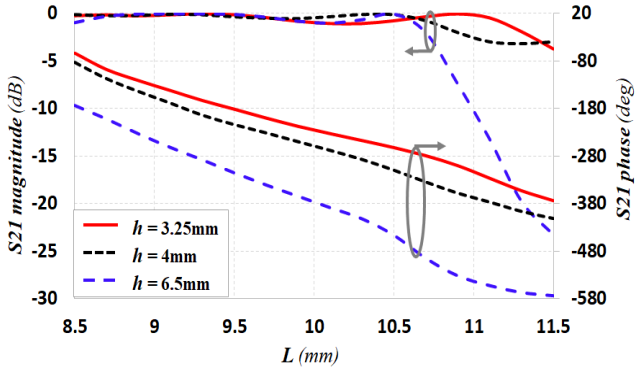

Fig. 6. Magnitude and phase of transmission coefficient versus L at 11.5GHz for h=3.25mm , h=4mm and h=6.5mm

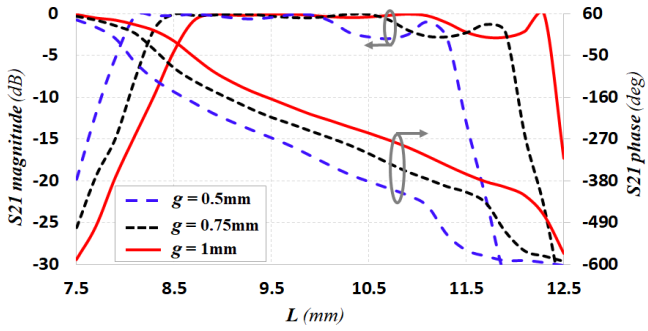

Fig. 7. Magnitude and phase of transmission coefficient versus L at 11.5GHz for g=0.5mm , g=0.75 and g=1mm

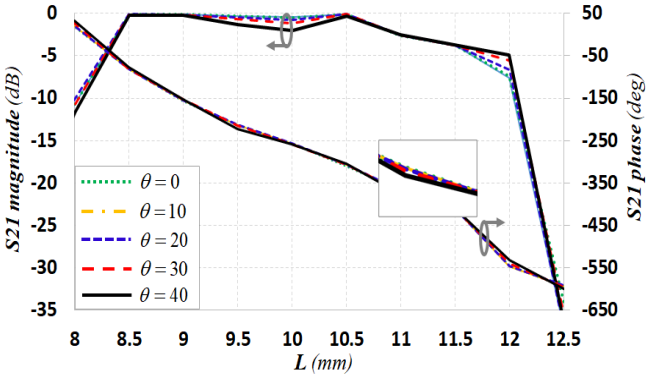

Fig. 8. Magnitude and phase of transmission coefficient versus L at 11.5GHz for various incidence wave angle, θ

This does not lead to a too thick structure, since h is chosen as one-sixth of the wavelength (lower than the commonly used value, a quarter of the wavelength).

Other cell parameters are denoted in Fig. 2a. For the proposed CSRR, P is designed based on the central frequency of the desired band and s provides the mechanical support for the structure with no significant impact on the transmission coefficient. Additionally, lower values of t are intended for the higher values of bandwidth. These parameters are optimized to P=12mm, t=0.1mm, and L=10mm to achieve a passband with the central frequency at 11.5GHz. This results in around 50% bandwidth as shown in Fig. 5.

Fig. 4 illustrates the phase-length curves versus L between 8.5 mm and 11.5 mm for the beginning, middle, and end frequency of the desired band. The curves approximately indicate linear behavior all over the range and demonstrate full phase coverage of 360 °.

L must be picked out from a range that is wide enough to give appropriate phase control and tight enough to spread the overlapped band.

Fig. 5 indicates the magnitude and phase of transmission coefficient in terms of frequency for L=9 mm, 10 mm, and 11mm. Perceived from this figure, in order to attain a symmetric overlapped bandwidth around 11.5 GHz, the slot length requires to vary from 9 mm to 11 mm. Therefore, L is considered to be 11 mm for the central element of the array, and it would be determined for other elements according to Fig. 4.

As a matter of fact, the passband frequencies impose a linear phase-frequency curve, as observed in Fig. 5. The transmission phase of the employed CSRR is highly sensitive to the slot length, making it an appropriate option for the array unit cell.

The figure also includes the transmission amplitude of the element demonstrating less than 3dB loss for all frequencies within the desired bandwidth. As shown in Fig. 5, the unit cell undergoes a considerable transmission loss for L= 11mm (L=9 mm) at the band upper (lower) frequencies.

It is noteworthy that a large range of slot length variation is demanded to reach phase control. However, it contradicts the wide overlapped passband of various L, as demonstrated from Fig. 5.

To evaluate the cross-polarization radiation of the proposed TA, Fig. 2d illustrates the tangential electric field (magnetic current) on the slot when the CSRR is exposed to an incident wave polarized parallel to the middle slot. As shown, the magnetic current extremely appears on the ring arms that are parallel to the incident magnetic field. Consequently, the re-transmitted wave has a low cross-polarization component.

As mentioned earlier, $h=\frac{\lambda}{6}$ is considered as an alternative for commonly used gap thickness which leads to a bulky structure for the current unit cell. Fig. 6 displays the transmission phase in terms of slot length at 11.5GHz for various h. While h=6.5 mm is more suitable to have a large phase gradient, h=4 mm yields the gradual phase variation required to have a wideband array and low-profile structure.

To evaluate the impact of g (indicated in Fig.2a), Fig. 7 is generated for which the magnitude and phase of transmission coefficient are depicted in terms of slot length. As shown, the range of slot length and passband of CSRR can be adjusted by g.

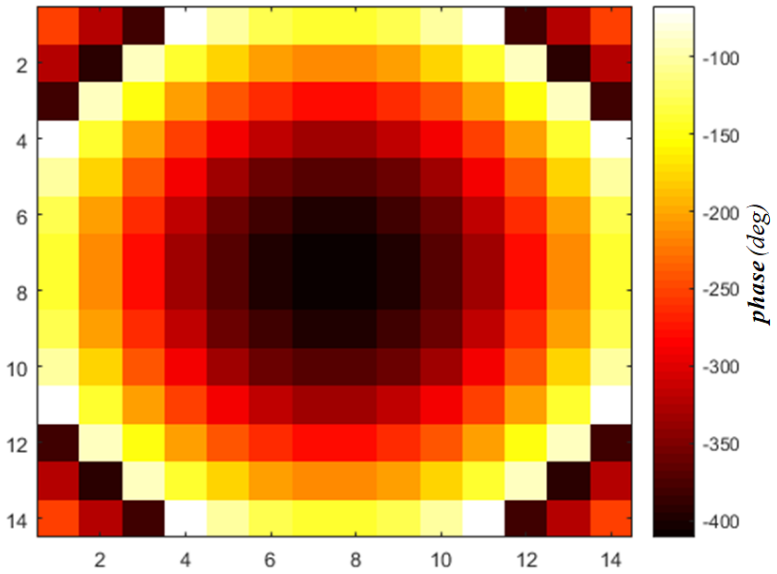

Fig. 9. Phase distribution pattern of elements on the array aperture

Having a uniform functionality necessitates the elements of the proposed array to keep the amplitude and phase curve of transmission coefficient unchanged for various incidence angles within a wide range of slot lengths. This is because the angle of the incident ray, θ, varies according to the array element position relative to the feed. Fig. 8 confirms a very high similarity for the amplitude and phase curves of the suggested unit cell for various θ between 0° and 40°. It is notable that incidence beam angles beyond $\theta = 30^\circ$, do not occur for any element since the focal length-to-diameter ratio $\frac{F}{D} = 1.1$ is considered for the current array.

4- Transmitarray Design

Using the previously suggested unit cell, a elements array is designed and manufactured $\frac{F}{D} = 1.1$ is chosen to compromise between aperture illumination efficiency (=spillover efficiency × tapering efficiency) and structure volume [12].

Elements of the array are illuminated by a pyramidal horn antenna having 13.5 dB gain at 11.5 GHz. The required compensating phase for each element based on its position in the array, is given by

$$\varphi_i = k(R_i - \vec{r}_i.\hat{r}_o) + \varphi_0 \qquad (1)$$

where k is the free space wavenumber, R_i is the distance of feed horn to i^{th} element, $\overline{r_i}$ is the position vector of i^{th} element, $\overline{r_o}$ is the unit vector of main beam, and φ_0 is a common phase constant for all elements. Fig. 8 illustrates the phase distribution pattern of elements on the array aperture. When the compensating phase is determined for each element by (1), the corresponding value of L would be found through the interpolation of the phase curve depicted in Fig. 4.

As shown in Fig. 4, transmission phase variation versus the slot length from 8.5 mm to 11 mm is descending, and less than 3-dB loss is observed at 11.5 GHz for the whole range. As mentioned earlier, L=1 mm is considered for the middle element of the array which prevents the sharp TA gain drop, as demonstrated in the following.

5- Simulation and Measurement Results

Fig. 10 shows the measurement setup in an anechoic chamber for the fabricated antenna. Simulation results are generated by Ansoft HFSS. E-plane and H-plane patterns for co/cross-polarization are indicated in Fig. 11 and Fig. 12, respectively, which show a good agreement between simulation and measurement results. The obtained side lobe and cross-polarization levels are -13 and -22 dB, respectively. The large value of SLL in this structure is due to the power spillover of the square array in the E-plane and H-plane. For example, SLL of -18 dB is obtained for the antenna pattern at $\varphi = 45^\circ$. Consequently, employing the circular array can improve the SLL significantly.To evaluate the radiation pattern over the frequency band, Fig. 13 depicts E-plane and H-plane patterns at 10.5GHz and 12.5GHz.

The antenna gains and aperture efficiency curves vs. frequency are also plotted in Fig. 14 for the simulation and measurement data. As can be seen, 1-dB and 3-dB gain bandwidth of 18.4% and 28% are attained by the measurement respectively, which is extremely high compared to previously reported values.

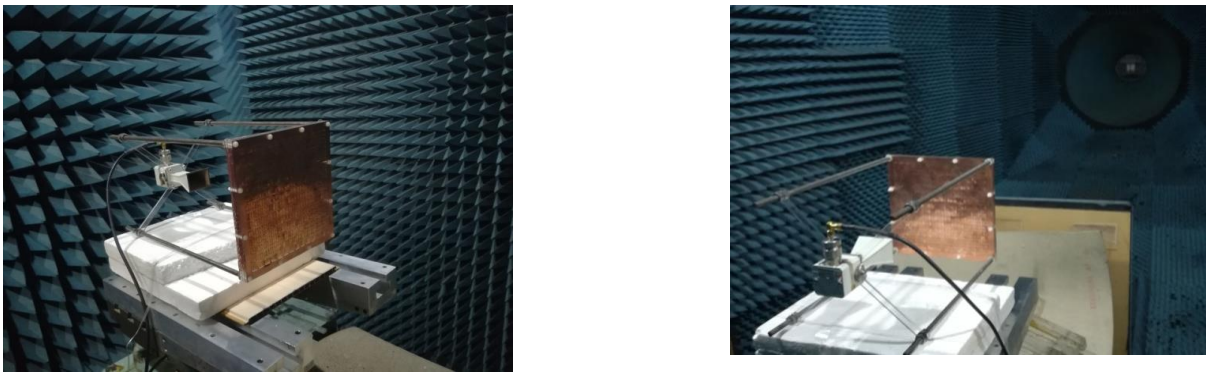

(a) (b)

Fig. 10. Measurement setup in an anechoic chamber for the fabricated Transmitarray Antenna. (a) front view, (b) back view

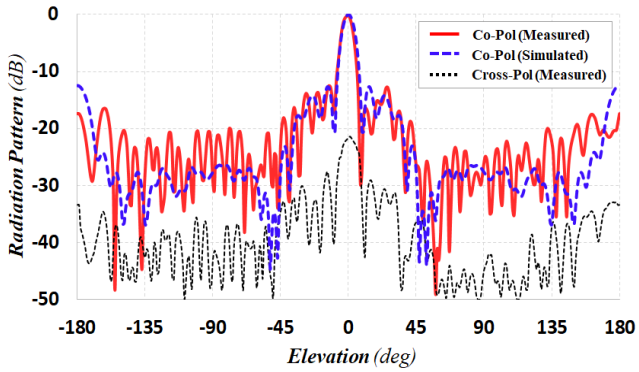

Fig. 11. E-plane radiation pattern of proposed transmitarray for co/cross-polarization

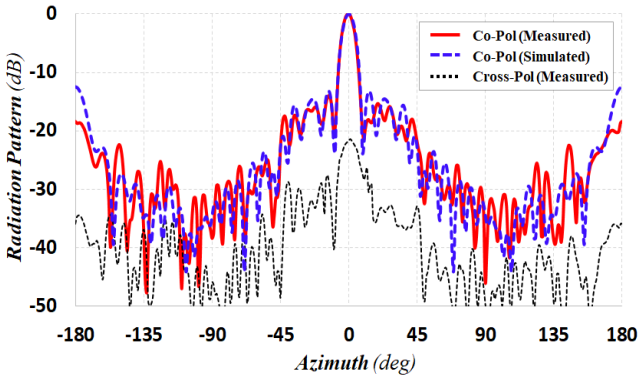

Fig. 12. H-plane radiation pattern of proposed transmitarray for co/cross-polarization

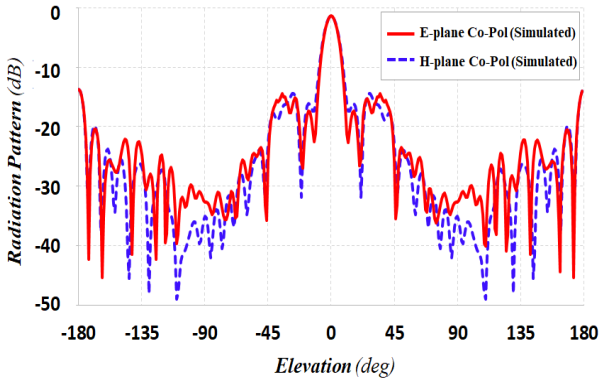

(a)

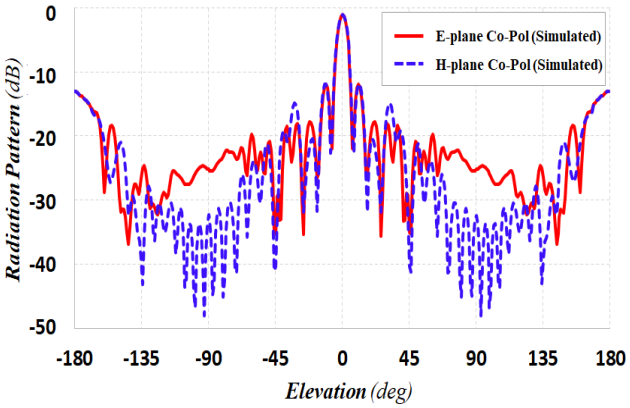

(b)

Fig. 13. Co-polarized E-plane and H-plane pattern at (a) 10.5GHz and (b) 12.5GHz

Table 1. Comparison of the current transmitarray array parameters with those reported in pervious works

Ref	f(GHz)	NL	MG	1-dB	3-dB	AE (%)	SLL (dB)	CPL (dB)
[1]	13.6	4	23.9	7.4	18.4	55	-19	-30
[2]	11.3	3	28.9	9	19.4	30	-19	-29
[3]	12	5	24.9	13.5	20	38.4	-20	-20
[4]	10.3	3	24.8	15.5	21	55	-24	-30
[5]	13.5	3	21	16	-	60	-15	-22
[6] (Ant 2)	13.5	4	-	11.7	29.3	47	-20	-30
[7]	10	3	25.9	7	20	-	-15	-
Prop. TA	11.5	4	24.6	18.4	28	53	-13	-22

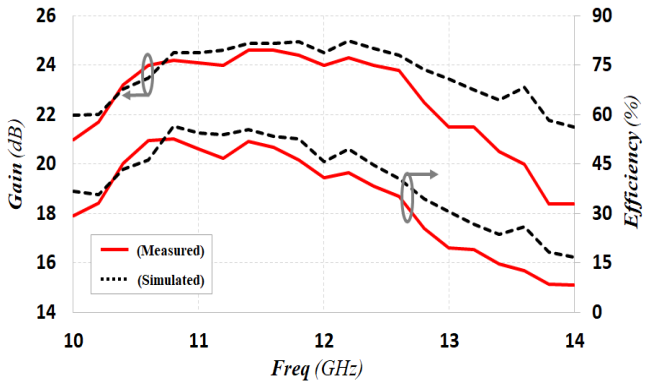

Fig. 14. Gain and aperture efficiency of proposed transmitarray in terms of frequency

It is noteworthy that the 3-dB band for the gain curve corresponds to the overlapped passband of the unit cell that is already obtained and confirms the proposed design procedure.

Moreover, maximum measured gain and aperture efficiency of 24.6 dB and 53% are observed at 11.5 GHz. These values have been achieved despite of relatively low feed horn gain. Various parameters of the current antenna, including the center frequency (f), Number of Layers (NL), Maximum Gain (MG), 1-dB and 3-dB Bandwidth (BW), Aperture Efficiency (AE), Side Lobe Level (SLL) and Cross-Polarization Level (CPL) are presented in Table 1 compared with ones reported in previous works.

6- Conclusion

In this paper, a procedure to design a wideband transmitarray is proposed and implemented for a TA based on a CSRR. It is demonstrated that the desired band needs to be enclosed in the overlapped passband of the unit cell for various slot lengths. This assures a low transmission loss over the specified band mostly for array central elements. The proposed CSRR also ascertains a low profile acquired by choosing $h=\frac{\lambda}{6}=4mm$ for the thickness of each layer. According to Table 1, the consequential parameters of the fabricated Transmitarray Antenna, including the maximum gain, aperture efficiency, and 1-dB and 3-dB bandwidth are placed at suitable positions compared to early researches. In the future, the prescribed approach in this paper could be well applied to the unit cells with higher bandwidth to increase the overlapped bandwidth of array elements.

References

[1] G. Liu, H.-j. Wang, J.-s. Jiang, F. Xue, and M. Yi, "A high-efficiency Transmitarray Antenna using double split-ring slot elements,"IEEE Antennas and Wireless Propagation Letters, 14 (2015) 1415-1418.

[2] A. H. Abdelrahman, A. Z. Elsherbeni, and F. Yang, "High-gain and broadband Transmitarray Antenna using triple-layer spiral dipole elements," IEEE Antennas and Wireless Propagation Letters, 13 (2014) 1288-1291.

[3] M. N. Jazi, M. R. Chaharmir, J. Shaker, and A. R. Sebak, "Broadband Transmitarray Antenna design using polarization-insensitive frequency selective surfaces," IEEE Transactions on Antennas and Propagation, 64 (2016) 99-108.

[4] B. Rahmati and H. Hassani, "High-efficient wideband slot Transmitarray Antenna," IEEE Transactions on Antennas and Propagation, 63 (2015) 5149-5155.

[5] Q. Luo, S. Gao, M. Sobhy, and X. Yang, "Wideband transmitarray with reduced profile," IEEE Antennas and Wireless Propagation Letters, 17 (2018) 450-453.

[6] A. H. Abdelrahman, P. Nayeri, A. Z. Elsherbeni, and F. Yang, "Bandwidth improvement methods of Transmitarray Antenna s," IEEE Transactions on Antennas and Propagation, 63 (2015) 2946-2954.

[7] K. Yan, X. Lv, Z. Han, and Y. Zhang. " Transmitarray Antenna with Double Conformal Rings as the Cell Elements." Applied Computational Electromagnetics Society Journal 34(7) (2019).

[8] M. –Y. Li, Y. –L. Ban and F. –Q. Yan, "Wideband Low-profile Ku-Band Transmitarray Antenna," IEEE Access, 9 (2021) 6683-6688.

[9] S. H. Ramazannia Tuloti, P. Rezaei and F. Tavakkol Hamedani, "High-Efficient Wideband Transmitarray Antenna," IEEE Antennas and Wireless Propagation Letters, 17(5) (2018) 817-820.

[10] W. Hu, J. Dong, Q. Luo, Y. Cai, X. Liu, L.Wen, W.Jiang, and S. Gao, " A Wideband Metal-Only Transmitarray With Two-Layer Configuration," IEEE Antennas and Wireless Propagation Letters, 20(7) (2021) 1347-1351.

[11] P. Feng, S. Qu, and S. Yang, "Ultrawideband Low-Profile Transmitarray With Vivaldi Array Feed," IEEE Transactions on Antennas and Propagation, 68(4) (2020) 3265-3270.

[12] Boccia, I. Russo, G. Amendola, and G. Di Massa, "Multilayer Antenna-Filter Antenna for Beam-Steering Transmit-Array Applications," IEEE Transactions on Microwave Theory and Techniques, 60(7) (2012) 2287-2300.

[13] J. Huang, "Reflectarray antenna," Wiley Online Library, (2008).

HOW TO CITE THIS ARTICLE

M R Salimi Beni, M Zoofaghari, A Wideband Transmitarray Antenna Design Based on the Transmission Characteristic of the Unit Cell, AUT J Electr Eng, 55(1) (2023) 3-10.

DOI: 10.22060/eej.2022.20591.5437